Vol. 14, No. 2: 1–23

# Fast and Stable Conformal Mapping Between a Disc and a Square

Michael M. Stark
Boise State University

**Abstract.** Mapping between a square or rectangle to a disc or hemisphere, and vice versa, arises in many areas of computer graphics, including environment and reflection mapping, sampling, and BRDFs to name a few. Different maps have different properties: equal-area maps may be more applicable in sampling, while low-distortion or continuity might be preferable in other applications. Conformal mapping preserves angles and thereby locally preserves shape. Although it has been used for over a century, conformal mapping between a disc and a square involves extensive computation with complex numbers. This paper reviews the construction of a conformal map between the unit disc and the unit square, which is formulated as an elliptic integral, and reviews several computational methods. Efficient algorithms are presented for mapping the disc to the square, and from the square to the disc. An implementation is provided in compact C language source code that runs at speeds comparable to simple trigonometric maps.

## 1. Introduction

The local behavior of a bijective planar map $F : \mathbb{R}^2 \to \mathbb{R}^2$, with $F(x, y) = (f_1(x, y), f_2(x, y))$, is determined by the Jacobian derivative matrix

$$J = \begin{bmatrix} \frac{\partial f_1}{\partial x} & \frac{\partial f_1}{\partial y} \\ \frac{\partial f_2}{\partial x} & \frac{\partial f_2}{\partial y} \end{bmatrix}.$$



1086-7651/09 $0.50 per page

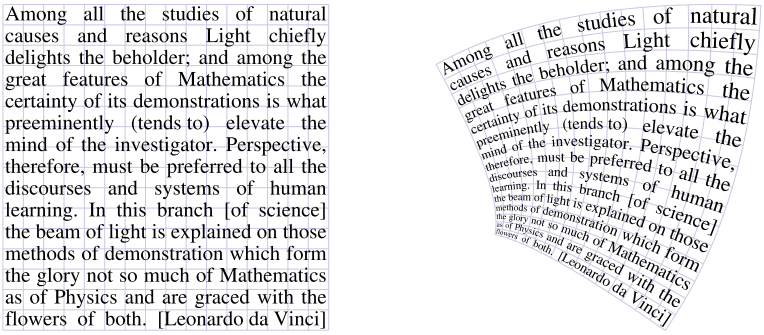


**Figure 1**. A conformal map preserves angles at the expense of distorting size.

The map is said to be *equal area* if the determinant $|J|$ is 1, and *conformal* if $J$ is a scaled rotation matrix. Informally, a conformal map is said to "preserve angles." That is, two curves in the domain of the map that meet at a conformal point get mapped, locally, to curves in the range that meet at the same angle. Conformal maps tend to preserve the basic shape of objects at the expense of distorting size. Figure 1 illustrates a simple conformal map from a square to another region. The Mercator projection, one of the most popular world map projections, is conformal: the basic shape of small regions is preserved but size is increasingly exaggerated toward the poles.

### *1.1. Complex Functions as Conformal Maps*

Expressed in rectangular coordinates, a complex number $z = x + iy$ has *real* part $x$, denoted by $\Re(z)$, and *imaginary* part $y$, denoted by $\Im(z)$. The complex numbers $\mathbb{C}$ can thus be visualized as a plane: each complex number $z = x+iy$ corresponds to a unique point $(x, y)$ in the Cartesian plane [Spiegel 64]. The $x$-axis corresponds to the real line, so it is often called the *real* axis. The $y$-axis is the *imaginary* axis. For the purposes of this work, the unit disc $D$ and the unit square $S$ are defined as subsets of the complex plane:

$$\begin{aligned} D &= \{z \in \mathbb{C} : |z| \leq 1\}, \\ S &= \{z \in \mathbb{C} : |\Re(z)|, |\Im(z)| \leq 1\}, \end{aligned} \tag{1}$$

where $|z| = |x+iy| = \sqrt{x^2 + y^2}$. The unit disc and unit square are illustrated in Figure 2, where grid lines are shown colored according to a standard coloring. A complex function $f : \mathbb{C} \to \mathbb{C}$ has the geometric interpretation of a map

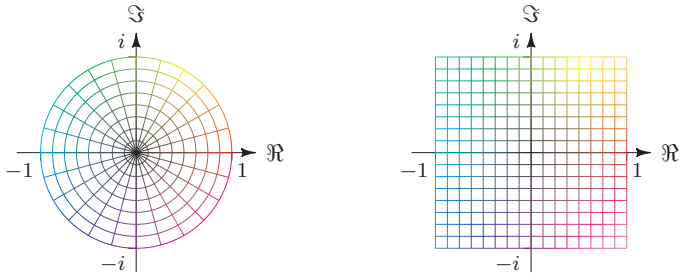


**Figure 2.** The unit disc and the unit square, drawn with grid lines in a standard coloring.

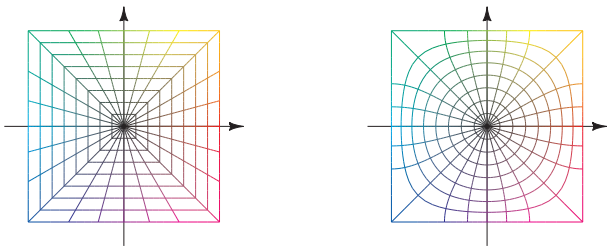

**Figure 3.** The unit disc transformed by Shirley's "warp" map (left) and the conformal map described in this paper (right). Shirley's map is not analytic as a complex function.

between two planes. One visualization of such a map is to display a collection of points or coordinate lines transformed by $f$. Figure 3 illustrates how the unit disc grid is transformed by Shirley's "warp" map [Shirley and Chiu 97] and the conformal map that is the subject of this paper.

Any complex function $f : \mathbb{C} \to \mathbb{C}$ analytic (infinitely differentiable) at a point $z_0$ with $f'(z_0) \neq 0$ is a conformal map in a neighborhood of $z_0$ [Spiegel 64]. Finding a conformal map from the disc to the square thus reduces to finding an appropriate complex analytic function. This problem is hardly new; in fact, it was considered a significant accomplishment when a hemisphere-to-square conformal map was developed through complex analysis [Grattan-Guinness 03].

This paper develops a conformal map from the unit disc $D$ to the unit square $S$, along with the inverse map, as complex functions. The map is derived in Section 2 and general evaluation techniques are discussed in Section 3. A reader primarily interested in implementing the maps might wish to skip these sections, or refer directly to Section 8.3 for the pseudocode.

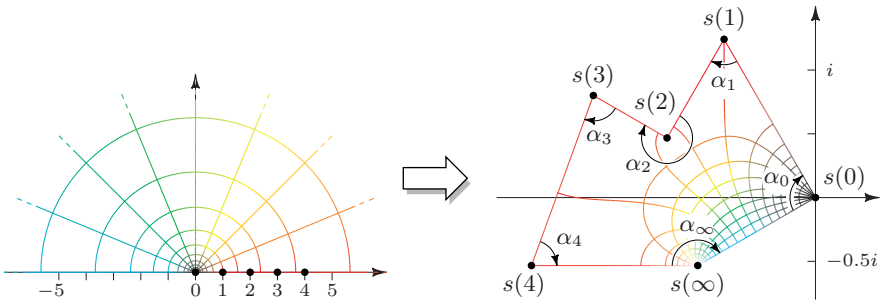


**Figure 4.** An example of the Schwarz-Christoffel map. Points $a_k$ on the real axis (in this case, $0, 1, 2, 3, 4$ and $\infty$) map to vertices of a polygon. The interior angle of the polygon at vertex $s(a_k)$ is $\alpha_k/\pi$. The point at infinity also maps to a vertex in this example.

## 2. Construction of the Disc-to-Square Conformal Map

The Schwarz-Christoffel transformation [Spiegel 64] provides an analytic function mapping the upper complex half-plane to a simply-connected polygon (i.e., one with no holes or self-intersections). Suppose $\alpha_1, \alpha_2, \ldots, \alpha_n$ are the interior angles of the polygon. Then for some constant $C$ and points $a_1 < a_2 < \cdots < a_n$ on the real axis, the function defined by the contour integral

$$s(z) = \int_0^z \frac{C}{(w-a_1)^{1-\alpha_1/\pi}(w-a_2)^{1-\alpha_2/\pi}\cdots(w-a_n)^{1-\alpha_n/\pi}}\, dw \qquad (2)$$

is an analytic function that maps the upper half-plane conformally onto a polygon having the specified interior angles. Figure 4 shows an example. Each point $a_k$ on the real axis maps to a unique vertex, which has an interior angle of $\alpha_k/\pi$. The real axis is continuously mapped to the boundary of the polygon. The point at infinity maps to one remaining vertex of interior angle $2\pi - \alpha_1/\pi - \alpha_2/\pi - \cdots - \alpha_n/\pi$, which is the angle needed to complete the polygon.

It is not difficult to see what makes the transformation work. Near $a_k$, $(w - a_k)$ is small and therefore the $1/(w - a_k)$ term dominates the integral:

$$s(z) \approx \int_0^z \frac{C'}{(w-a_k)^{1-\alpha_k/\pi}} = \frac{C'}{\alpha_k/\pi}(z-a_k)^{\alpha_k/\pi}.$$

The function $(z-a_k)^{\alpha_k/\pi}$ has the effect of "bending" the real line to an angle of $\alpha_k/\pi$ at $z = a_k$, i.e., to a polygon vertex (Figure 5).

Although it has an elegant formulation, the Schwarz-Christoffel transformation is not easy to use in practice. The formula of (2) does not apply

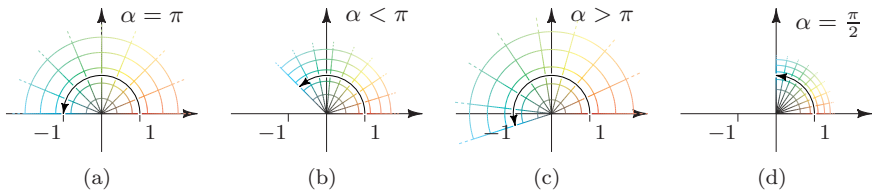


**Figure 5**. The function $z^{\alpha/\pi}$ has the effect of bending the upper half-plane to angle $\alpha$ at the origin. (a) When $\alpha = \pi$, it reduces to the identity function. Otherwise the bend produces a convex (b) or concave (c) vertex. (d) If $\alpha = \pi/2$, $z^{\alpha/\pi} = \sqrt{z}$, which suggests how the half-plane can be bent into a square.

directly to an arbitrary predefined polygon: it only assures a map to *some* polygon having the supplied vertex angles. The points $a_k$, the constant $C$, and the integration constant have to be judiciously chosen in order to map to a particular polygon. Furthermore, the integral defining the map has to be evaluated at each point on which the transformation is applied. Only in the simplest cases can an anti-derivative be found. In most cases, including the transformation to a square, numerical methods are required for evaluation.

### *2.1. Schwarz-Christoffel Mapping to the Square*

Constructing a Schwarz-Christoffel map from the upper half-plane to a square (Figure 6) is a common example or exercise in complex analysis texts

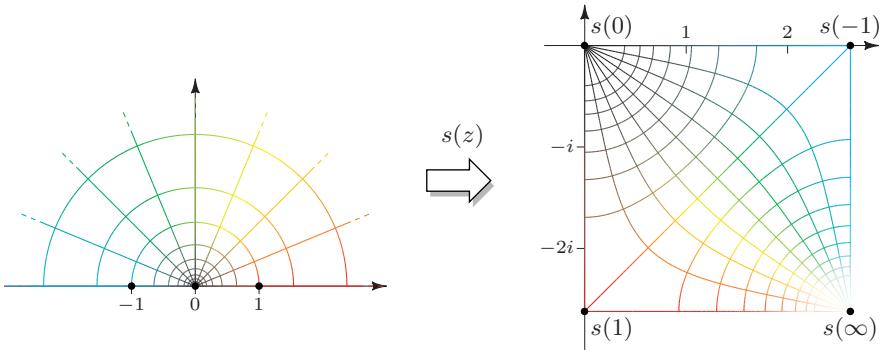


**Figure 6**. The Schwarz-Christoffel map to the square upon which the disc-to-square map is based. Note the symmetry that results from choosing vertex antecedents that are symmetric about the origin.

(e.g., [Churchill and Brown 90, Spiegel 64]). One way is to use the integral

$$s(z) = \int_0^z \frac{1}{\sqrt{w(w-1)(w+1)}}\, dw. \tag{3}$$

The singularities in the integrand, $z = -1, 0, 1, \infty$, map to vertices of the square. Complex analysis texts tend to leave it at that: the actual (square) range of the map and how to evaluate it in practice are seldom considered. The "unnormalized" square range of (3) needs to be translated and scaled to match the unit square $S$ as defined in (1). But first a conformal map from the disc to the half-plane is needed to compose with (3) for a disc-to-square map.

### *2.2. From the Disc to the Square*

The Möbius transformation [Needham 99]

$$w(z) = i\frac{1-z}{1+z} \tag{4}$$

maps the unit disc to the upper half-plane, and therefore the composite map $s(w(z))$ maps the unit disc to a square (Figure 7). Applying a change of variable in (4) results in a map from the disc to an unnormalized square:

$$s(w(z)) = \int_1^z \frac{\sqrt{-2i}}{\sqrt{(1-\zeta^2)(1+\zeta^2)}}\, d\zeta. \tag{5}$$

The constant $\sqrt{2i}$ has the effect of scaling and rotating the square, and the lower integration limit only changes the position; therefore, the integral

$$I(z) \equiv \int_0^z \frac{1}{\sqrt{(1-\zeta^2)(1+\zeta^2)}}\, d\zeta \tag{6}$$

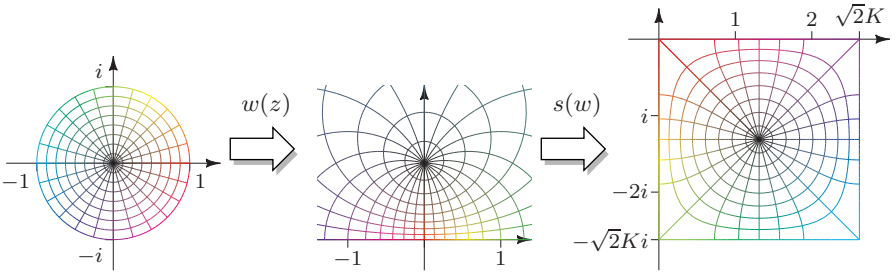


**Figure 7.** The function $w(z)$ maps the unit disc to the upper half-plane; the composition $s(w(z))$ maps the unit disc to a square.

also provides a map from the disc to a (different) square, illustrated in Figure 8(a). The map is confirmal since $I'(z) \neq 0$ inside the disc. Because its formulation is simpler than (5), $I(z)$ is regarded as the basic disc-to-square integral in this work. Much of the rest of this paper is concerned with its efficient evaluation.

### *2.3. Transforming the Square*

The final step in the construction is to transform the unnormalized square $I(D)$ to the unit square $S$. The process is illustrated in Figure 8. The antecedents of the vertices of the square are necessarily the singular points of the integrand of $I$, which lie at $z = \pm 1, \pm i$. Since $I$ is an odd function ($I(-z) = -I(z)$), the vertices are $-I(1)$, $I(1)$, $-I(i)$, $I(i)$. Vertices $-I(1)$ and $I(1)$ lie on the real axis, as the integrand of $I$ is real for $-1 \leq \zeta \leq 1$. The square $I(D)$ thus has its main diagonals on the coordinate axes and is inscribed in a circle of radius $I(1)$. Multiplying by $\sqrt{2}/I(1)$ scales the square to the proper size; multiplying by $\sqrt{-i}$ rotates by $-45°$ (Figure 8(b)).

Although it is not strictly necessary, it seems reasonable to require $f(z) \approx z$ near $z = 0$, so that the map is minimally deforming at the center of the disc. Rotating $z$ by 45°, which can be effected by multiplying by $\sqrt{i}$, accomplishes this (Figure 8(c)). The final disc-to-square map is thus $s(w(\sqrt{i}\, z))$ scaled by the semi-side length:

$$f(z) \;\equiv\; \frac{\sqrt{-2i}}{I(1)}\, I\left(\sqrt{i}\, z\right) \;=\; \frac{2\sqrt{-i}}{K}\, I\left(\sqrt{i}\, z\right);$$

$I(1) = K/\sqrt{2}$; the value of $K$ is given in (8). It follows from the Riemann mapping theorem, an important result in complex analysis [Churchill and

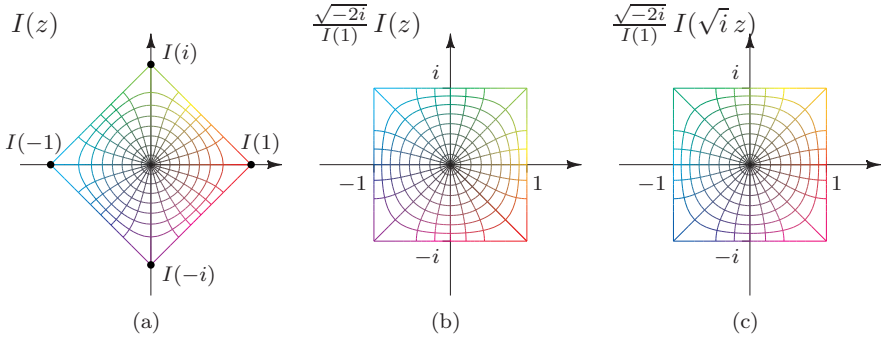


**Figure 8.** (a) The function $I(z)$ maps the unit disc to a square centered at the origin. (b) Multiplying by $\sqrt{-2i}/I(1)$ scales and rotates to the unit square. (c) Multiplying $z$ by $\sqrt{i}$ pre-rotates to provide a unit derivative at the origin.

Brown 90], that the disc-to-square conformal map is unique once the angle at 0 is chosen.

### *2.4. The Transformation as an Elliptic Integral*

The integral $I(z)$ of (6) cannot be evaluated in closed form. Nevertheless, it is an *elliptic integral*, a class of well studied integrals for which there are effective numerical evaluation techniques [Abramowitz and Stegun 64]. The first step in applying these techniques is to reduce the integral to one of three canonical forms. By a stroke of luck, $I(z)$ is already in canonical form: the *incomplete elliptic integral of the first kind* is defined as

$$F(\phi|m) = \int_0^z \frac{1}{\sqrt{(1-t^2)(1-mt^2)}}\, dt,$$

where $\phi$, known as the *amplitude*, satisfies $\sin\phi = z$. In $I(z)$, $m = -1$:

$$I(z) = F(\phi|-1).$$

Standard numerical methods require that $m$, known as the *parameter*[1] of the elliptic integral, satisfies $0 < m \leq 1$. A formula to reduce a negative parameter [Abramowitz and Stegun 64] produces

$$F(\phi|-1) = \frac{1}{\sqrt{2}} F\left(\frac{\pi}{2}\middle|\frac{1}{2}\right) - \frac{1}{\sqrt{2}} F\left(\frac{\pi}{2} - \phi\middle|\frac{1}{2}\right)$$

and thereby yields the final form of the disc-to-square conformal map

$$f(z) = \sqrt{-i}\,\frac{K}{2} - \sqrt{-i}\, F\left(\frac{\pi}{2} - \arcsin\sqrt{i}\, z\middle|\frac{1}{2}\right). \tag{7}$$

The value $K$ is known as the *complete elliptic integral*;

$$K = F\left(\frac{\pi}{2}\middle|\frac{1}{2}\right) \approx 1.854074677301372, \tag{8}$$

and $\sqrt{i} = \frac{1}{\sqrt{2}}(1+i)$, $\sqrt{-i} = \frac{1}{\sqrt{2}}(1-i)$.

[1]The quantity supplied by the parameter $m$ can also be expressed in terms of the *modulus* $k$, with $k^2 = m$, or the *modular angle* $\alpha$, with $\sin\alpha = k$. Traditional notation for elliptic integrals uses the delimiters "|", ",", and "\" to indicate the second argument is, respectively, the parameter, modulus, or modular angle; i.e., $F(\phi|m) \equiv F(\phi, \sqrt{m}) \equiv F(\phi\backslash \arcsin\sqrt{m})$.

## 3. Evaluation of Elliptic Integrals

Evaluation of the formula given in (7) hinges on the computation of the incomplete elliptic integral function $F$. Elliptic integrals show up often enough that code for computing $F$ is available in many existing numerical software libraries. For example, the GNU Scientific Library provides functions for evaluating $F$, but only for real values. Computing $F$ for complex values, as is needed for (7), is significantly more complicated. On the other hand, evaluation of (7) is restricted to a fixed parameter $m = 1/2$ and known bounds on $\phi$, which makes the evaluation somewhat simpler. Using a general evaluator for $F$ is not only overkill, it is potentially wasteful.

### *3.1. Landen Transformations*

Landen's *ascending* transformation can be used to compute $F$ by replacing $\phi$ and $m$ with values $\phi'$ and $m'$ so that $F(\phi|m) = F(\phi'|m')$ and $m < m'$. When $m$ is sufficiently close to 1, a special-case formula can be applied. To compute $F(\phi|m)$, start with

$$\zeta_0 = 1, \quad k_0 = \sqrt{m}, \quad \phi_0 = \phi,$$

then compute

$$\phi_{j+1} = \frac{\arcsin(k_j \sin\phi_j) + \phi_j}{2}, \quad k_{j+1} = \sqrt{1 - \left(\frac{1-k_j}{1+k_j}\right)^2}, \quad \zeta_{j+1} = k_{j+1}\zeta_j.$$

As $n$ increases,

$$F(\phi|m) \to \sqrt{\frac{\zeta_n}{\sqrt{m}}} \ln\left(\tan\left(\frac{\pi}{4} + \frac{\phi_n}{2}\right)\right).$$

The convergence is quadratic: for double-precision values in (7), at most six iterations are needed; for single-precision values, four iterations suffice.

Landen's *descending* transformation works similarly, but is not as well suited to this particular evaluation, despite having a slightly simpler formulation. Landen transformations work for complex arguments as well as real arguments, but in the complex case appropriate branches of the multi-valued inverse trigonometric functions have to be tracked. Both Landen transformations seem stable in quadrant IV for evaluation of (7). This is sufficient, as the map is symmetric and the other quadrants can be transformed to and from this quadrant.

### 3.2. The Arithmetic–Geometric Mean

Given two initial values $a_0$ and $b_0$, the *arithmetic–geometric mean* (AGM) is the double sequence $a_j$, $b_j$ computed inductively, as the name implies, from

$$a_{j+1} = \frac{a_j + b_j}{2}, \quad b_{j+1} = \sqrt{a_j b_j}.$$

The sequences converge quadratically to a common value. To compute $F(\phi|m)$ using the AGM, start with

$$a_0 = 1, \quad b_0 = \sqrt{1-m}, \quad \phi_0 = \phi$$

and for each $j = 0, 1, 2, \ldots$, compute $a_{j+1}$, $b_{j+1}$ from (3.2), along with

$$\phi_{j+1} = \phi_j + \arctan\left(\frac{b_{j+1}}{a_{j+1}} \tan\phi_j\right). \tag{9}$$

Then as $n$ increases,

$$F(\phi|m) \to \frac{\phi_n + q_n \pi}{2^n a_n} \tag{10}$$

for an appropriate integer $q_n$. As (10) suggests, the value of $q_n$ has to chosen so that the difference $\phi_{j+1} - \phi_j$ stays near $2^n$. The problem of computing $q_n$ is examined in Section 4.2.

### 3.3. Carlson's Formulation

Elliptic integrals here follow the "classical" treatment. A reformulation of elliptic integrals due to Carlson [Press et al. 92] has the advantage of unifying all three kinds in one form and provides a single numerical method for all three. While this is a significant accomplishment for general computation, Carlson's approach does not seem to be particularly beneficial to the map discussed in this paper.

### 3.4. Reduction to Real Arguments

The computation of $F$ for a complex argument can be reduced to $F$ evaluated on two real arguments [Abramowitz and Stegun 64]:

$$F\left(\phi + i\psi|\tfrac{1}{2}\right) = F\left(\lambda|\tfrac{1}{2}\right) + i\,F\left(\mu|\tfrac{1}{2}\right) \tag{11}$$

where, if $b = 2\cot^2\phi + \sinh^2\psi \csc^2\phi - 1$,

$$\cot^2\lambda = \frac{b + \sqrt{b^2 + 8\cot^2\phi}}{4}, \tag{12}$$

$$\tan^2\mu = 2(\tan^2\phi\,\cot^2\lambda - 1). \tag{13}$$

To apply this to (7) the real and complex parts of $\pi/2 - \arcsin\sqrt{i}\,z$ are needed explicitly. If $\sqrt{i}\,z = x + iy$, then with the appropriate branch of the inverse sine

$$\phi + i\psi = \frac{\pi}{2} - \arcsin(x + iy) = \arccos\beta - i\ln\gamma,$$

where

$$\alpha = \frac{A+B}{2}, \quad \beta = \frac{A-B}{2}, \quad \gamma = \alpha + \sqrt{\alpha^2 - 1},$$

with $A = \sqrt{(x+1)^2 + y^2}$ and $B = \sqrt{(x-1)^2 + y^2}$. Some simplification gives

$$\tan^2\phi = \frac{1-\beta^2}{\beta^2}, \quad \csc^2\phi = \frac{1}{1-\beta^2}, \quad \sinh^2\psi = \frac{1}{4}\left(\gamma - \frac{1}{\gamma}\right)^2,$$

which can be substituted directly into (12) and (13) to obtain $\lambda$ and $\mu$. Then (11) can be applied, with $F$ computed using the method of choice.

## 4. Practical Evaluation and Stability Considerations

Computing $F$ on real and imaginary parts separately via the real reduction of Section (3.4) is typically faster than using Landen transformations or the AGM with complex arithmetic. But, as with the other methods of computing $F$, the reduction is more complicated than it might appear. Getting the right signs of $\cot\lambda$ and $\tan\mu$ in (12) requires a maze of conditional statements, and choosing the proper branches of the inverse trigonometric functions can be tricky. Furthermore, the real argument reduction is fraught with instabilities, primarily due to the radicals. It is particularly troublesome when $y$ is small compared with $x$, or vice versa. This section is concerned with the development of a stable, practical algorithm for the disc-to-square conformal map. Most of the stability issues can be resolved by splitting the disc into separate regions, in which appropriate computational methods can be applied (Figure 9).

The square symmetry of the map offers some flexibility in the computation: an algorithm (or choice of signs) that is stable in one octant suffices for the entire disc. Away from the real axis, the real reduction of (11) and the AGM algorithm behave well in the octant with $0 \le x$, $-x < y \le 0$ if positive roots and principal branches of the inverse functions are taken. A power series expansion is developed in the next subsection that can be used to cover the real axis, thereby avoiding most of the trouble spots of the real reduction and AGM. Unless otherwise stated, the expressions in this section assume "$z$" is actually $\sqrt{i}\,z$ in the context of (7), i.e., $z$ has already been rotated. Attention is given to the restriction of the (rotated) disc to Quadrant IV, illustrated in Figure 9(b).

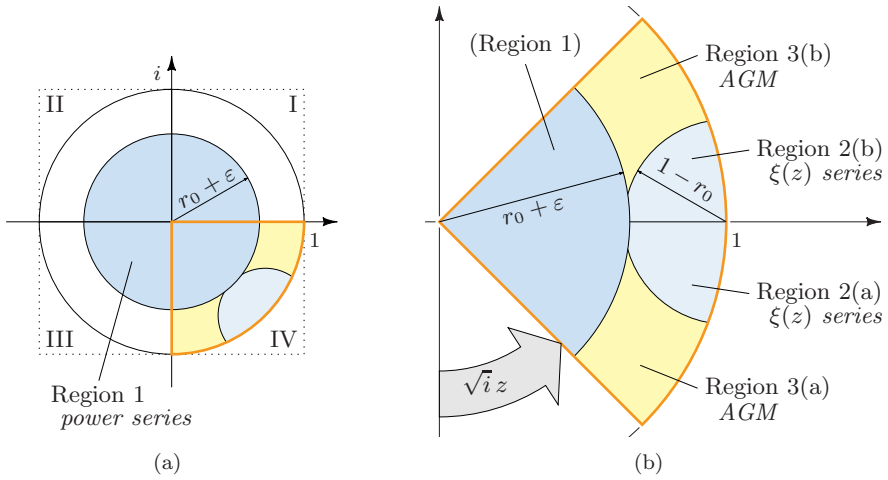


**Figure 9.** The best method for computing $F(\sqrt{i}\,z)$ depends on where $z$ lies in the domain. (a) The power series works best for $z$ near the center (Region 1), but requires too many terms as $|z| \to 1$. (b) All other regions can be reduced to Quadrant IV, which, when rotated by $\sqrt{i}$, is symmetric about the real axis. Near $z = 1$ (Region 2), the series can be applied to $\xi(z)$. Elsewhere the AGM algorithm is used (Regions 3(a) and 3(b)). The minimal radius $r_0$ of Region 1 is expanded by $\varepsilon$ so that Region 1 and Region 2 overlap, keeping Regions 3 away from the real axis.

### *4.1. A Series Expansion*

The integrand of $I(z)$, from (6), can be expanded as a binomial series

$$\frac{1}{\sqrt{(1-\zeta^2)(1+\zeta^2)}} = (1-\zeta^4)^{-1/2} = \sum_{n=0}^{\infty} \frac{(2n-1)!!}{2^n n!}\zeta^{4n},$$

which converges absolutely for $|\zeta| < 1$. Term-by-term integration gives

$$I(z) = \int_0^z \frac{1}{\sqrt{(1-\zeta^2)(1+\zeta^2)}}\, d\zeta = z\sum_{n=0}^{\infty} \frac{(2n-1)!!}{(4n+1)2^n n!} z^{4n}, \tag{14}$$

which converges for $|z| < 1$. The convergence is rapid for fairly small $z$, but requires prohibitively many terms for $|z|$ near 1. The region in which the power series is useful is a disc and is described hereafter as *Region 1*. The `SumSeries` function given in Section 8.3 shows how (14) can be summed to a specific number of terms by incrementally computing the series coefficients. The implementation in the source code provided uses Horner's scheme ([Press et al. 92]) with precomputed coefficient values to evaluate the summation.

A property of the disc-to-square integral allows the series expansion to be applied at $z = 1$, which eliminates another stability problem. If

$$\xi(z) = \sqrt{\frac{1 - z^2}{1 + z^2}}$$

a change of variables in (6) results in the formula

$$I(z) = \frac{K}{\sqrt{2}} - I(\xi(z)).$$

The geometry of the transformation is illustrated in Figure 10. Because $\xi(1) = 0$, the computation at 1 can thus be "flipped" to 0 by applying the power series of (14) to $\xi(z)$. In fact, the positive real axis inside the disc can be covered by combining the use of the series of $z$ and $\xi(z)$. The point of overlap occurs when $\xi(r_0) = r_0$, which is

$$r_0 = \sqrt{\sqrt{2} - 1} \approx 0.6436.$$

The $\xi(z)$ transformation makes the power series applicable in the inverse image of Region 1, which is described as *Region 2*. Points $z$ in Region 2 must satisfy $|\xi(z)| < r_0$ in order to cover the real axis. The minimal radius $r_0$ of Region 1 must be expanded slightly to $r_0 + \varepsilon$ so that Regions 1 and 2 overlap, in order to assure the inclusion of values of $z$ near the real axis; $\varepsilon = 0.02$ is a reasonable choice. The maximum number of series terms needed for $|z| < r_0 + 0.02$ is 18 for double-precision arithmetic, and 8 for single-precision arithmetic.

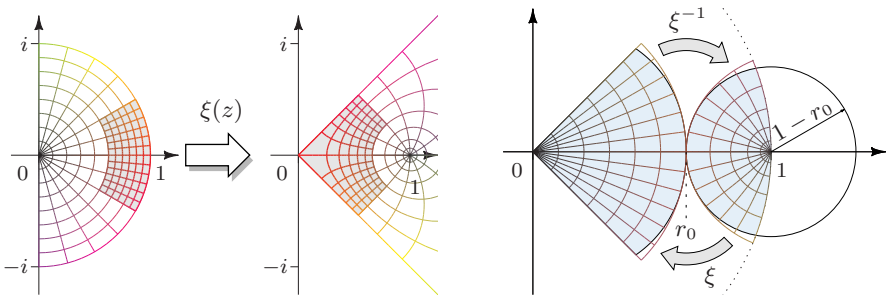


(a) (b)

**Figure 10.** (a) The effect of the "flip" function $\xi(z)$ on the right semidisc: the bounding circle is transformed to straight lines meeting at a right angle, with $\xi(1) = 0$ at the vertex. (b) The point $r_0$ is the fixed-point $\xi(r_0) = r_0$. The sector of the circle of radius $r_0$ is transformed by $\xi^{-1}$ to a region roughly the shape of a disc of radius $1 - r_0$ centered at 1 (and clipped against the unit disc).

Figure 10(b) shows that the disc of radius $1 - r_0 = r_1$ centered at 1 is transformed by $\xi$ to a region approximately bounded by $r_0$. (It is not visible in the figure, but the transformed region "bulges out" slightly, so it is not quite bounded by $r_0$.) Region 2 is thus well approximated by this disc. Equating Region 2 with this disc simplifies the containment test, as it eliminates the evaluation of $\xi(z)$.

### *4.2. An Optimized AGM Algorithm*

The regions of (rotated) Quadrant IV not included in Regions 1 and 2 are described as *Region 3(a)* and *3(b)* (Figure 9(b)). The real reduction and AGM algorithm work well in Region 3(a) below the real axis. The AGM algorithm can be optimized by operating on the tangents of the $\phi_j$ rather than on the angles $\phi_j$. The crux of the algorithm, given in (9), can be reformulated using the tangent-sum identity:

$$\tan \phi_{j+1} = \frac{(b_j + a_j) \tan \phi_j}{a_j - b_j \tan^2 \phi_j},$$

In the real reduction given by (11), the values of $\mu$ and $\lambda$ are computed from their tangents. Passing $\tan \mu$ and $\tan \lambda$ directly to the AGM algorithm eliminates *all* trigonometric function evaluations until the evaluation of (10), which becomes

$$F\big(\phi|\tfrac{1}{2}\big) = \frac{\arctan(\tan \phi_n) + q_n \pi}{2^n a_n}. \tag{15}$$

For double-precision arithmetic, four iterations ($n = 4$) suffice; for single-precision, $n = 3$ is enough. The values of the AGM sequence $a_j$ and $b_j$ do not depend on $\phi$ and can be precomputed. Values up to $n = 4$ are given in Table 1. On contemporary hardware, though, just computing $a_j$ and $b_j$ along with $\tan \phi_j$ might be preferable to a table lookup.

The value of $q_n$, which represents the branch of the inverse tangent, is more difficult to track when tangents are used in place of angles. However, because $q_n$ is an integer, the error induced by an incorrect value of $q_n$ is a

| $j$ | $a_j$ | $b_j$ |
|---|---|---|
| 0 | 1.0000000000000000 | 0.7071067811865475 |
| 1 | 0.8535533905932737 | 0.8408964152537145 |
| 2 | 0.8472249029234942 | 0.8472012667468914 |
| 3 | 0.8472130848351929 | 0.8472130847527654 |
| 4 | 0.8472130847939792 | 0.8472130847939792 |

**Table 1**. Values of the AGM. Note the rapid convergence.

multiple of $\pi/(2^n a_n)$. The value of $q_n$ can be computed from a sufficiently accurate approximation to $F$ by rounding. The following formula is developed in Section 8.1:

$$q_n = \left\lfloor \frac{1}{2} + \frac{2^n a_n \tilde{F}(\tan\phi_0) - \phi_n}{\pi} \right\rfloor,$$

where

$$\tilde{F}(\tan\phi_0) = \tan\phi_0 - 0.193\,(\tan\phi_0)^3 + 0.026\,(\tan\phi_0)^5$$

is an approximation to $F\big(\phi_0|\frac{1}{2}\big)$.

### *4.3. Evaluation Algorithm*

The complete disc-to-square conformal map algorithm is collected in Algorithm 3 (Section 8.3). The basic process is to apply the central series summation of (14) for $|z| < r_0 + \varepsilon$, otherwise rotate to Quadrant IV, and either use the series on $\xi(z)$ if $|\xi(z)| < r_0$, or the optimized AGM algorithm with the real-argument reduction.

The source code provided contains an optimized implementation of this algorithm. Most notably, speedup is obtained by minimizing the number of summed terms in the power series. As noted previously, 18 terms suffice for $|z| < r_0$ (in double-precision arithmetic), but far fewer terms are needed for smaller $z$. Figure 11(a) contains a plot of the number of terms required as a function of $|z|$. An empirical upper bound on the number of terms required is $\lfloor (3.48 + 6.65|z| - 3.19|z|^2)/(1 - |z|) \rfloor$, but $\lfloor 6.5/(1 - |z|) - 2 \rfloor$ works fine in practice.

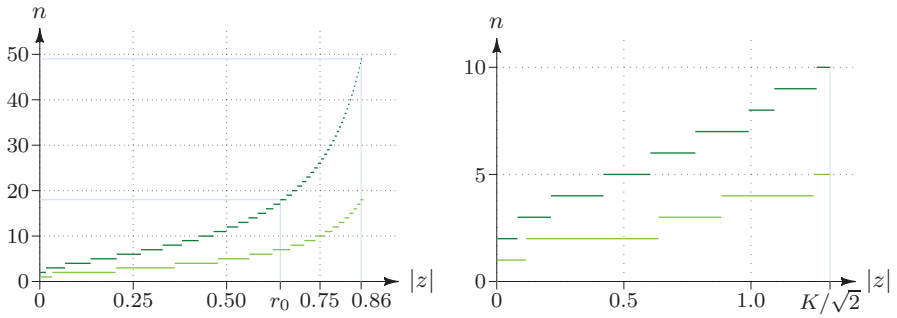


(a) Required Terms of the $I(z)$ Series (b) Required Terms of the Inverse Series

**Figure 11**. Number of terms required for the series expansions as functions of $|z|$, for single- and double-precision arithmetic (light and dark green, respectively).

The power series is computationally superior to the AGM algorithm for several reasons: it is faster, more stable, and does not require a real-argument reduction. However, the speed decreases as the number of terms summed increases. For sufficiently large $|z|$, the AGM algorithm is a better choice. Experiments have shown that the series implementation runs faster than the AGM implementation when up to about 50 terms are included (although this is highly dependent on the CPU), which corresponds to a radius of about $r_0 = 0.86$. Region 2 is also implicitly expanded when $r_0$ is increased. An empirically determined formula for the radius $r_1$ of a disc to approximate Region 2, to match the number of terms in Region 1, is $r_1^2 = 0.46 - 1.67r_0 + 1.79r_0^2$.

## 5. Inversion: A Conformal Map from the Square to the Disc

The inverse of the conformal map from the disc to the square is a conformal map from the square to the disc. The inverse of the disc-to-square function $f(z)$ can be expressed in terms of the inverse of $I(z)$. Setting $w = f(z)$ and solving for $z$ in (7) produces a formula in terms of the inverse of $I(z)$:

$$f^{-1}(w) = \frac{1}{\sqrt{i}}\, I^{-1}\left(\frac{Kw}{2\sqrt{-i}}\right).$$

Inverses of elliptic integrals are Jacobi elliptic functions, which are studied and applied at least as much as elliptic integrals. Modifications of Landen's transformations or the AGM algorithm can be used for efficient computation.

As it happens, inversion of $I(z)$ can be expressed as a rational function and a rapidly converging power series. The series expansion of (14) can be inverted directly to provide a series for $I^{-1}(w)$. (Numeric values for the coefficients are included in the source code.) Unlike the series expansion for $I(z)$, the entire unit square is well inside the radius of convergence of the inverse series. In fact, 30 or so terms (at most) are sufficient to compute the inverse map.

A trick can be employed to accelerate the convergence. Examination of the inverse series coefficients shows that for large $j$ the $j$th term is approximately

$$(-1)^j C_0 K^{-4(j+1)}, \quad C_0 \approx 13.750371636040937$$

(the meaning of the empirically determined constant $C_0$ is unclear). Tails of the series thus approximate a geometric series; subtracting the sum of this series results in a different series expansion:

$$I^{-1}(w) \approx \frac{C_0 w}{K^4 + w^4} + w\left(c_1 + c_5 w^4 + c_9 w^8 + \cdots\right).$$

The coefficients $c_j$, which are given in Table 2, drop to zero much faster than those of the ordinary inverse series. At most 10 terms are needed for the entire

| $k$ | $c_k$ | $k$ | $c_k$ |
|---|---|---|---|
| 1 | $-1.6360491363469976\times10^{-01}$ | 21 | $-1.4786423004927015\times10^{-13}$ |
| 5 | $-1.5316508620083077\times10^{-03}$ | 25 | $-6.1034023099548599\times10^{-16}$ |
| 9 | $+5.9455890307966153\times10^{-07}$ | 29 | $+5.3527850055041484\times10^{-19}$ |
| 13 | $+1.7520282395125552\times10^{-08}$ | 33 | $+7.9773298274614004\times10^{-21}$ |
| 17 | $+2.8997255626121623\times10^{-11}$ | 37 | $+1.1683926152311516\times10^{-23}$ |

**Table 2**. Coefficients for the inverse (square-to-disc) series.

square, including the boundary. Figure 11(b) contains a plot of the required number of terms.

## 6. Stability Analysis

One empirical approach to checking the numerical stability of the disc-to-square and square-to-disc algorithms is to map a point $z$ from the disc to the square, then map it back to the disc. The difference, i.e., $|z - f^{-1}(f(z))|$ is a reasonable test of numerical accuracy (the two algorithms are sufficiently different in operation that precision errors in the forward algorithm are not likely to be canceled by corresponding errors in the inverse algorithm). Table 3 lists computed values of $\max|z_k - f^{-1}(f(z_k))|$ by domain region. The values were computed using the implementation provided, on some $10^{10}$ points $z_k$ distributed across the disc. The error exhibited in Regions 1 and 3 is within a factor of 10 of the floating-point epsilon.

The only notable stability problem occurs in Region 2 and is a result of loss of precision in $\xi$ when $\sqrt{i}\,z = x + i\delta$ for small $\delta$, i.e., near one of the main diagonals of the square. This problem can be eliminated by using series expansions given in Section 8.2. Implementing them is not likely to be worth the trouble though, because the error is not significant in practice. For example, if the algorithms were employed to create a poster-sized image, the error in the single-precision case would be less than the dot pitch of a 2400 DPI printer; in the double-precision case, the error would be at the atomic scale.

| | Max Error (single-prec.) | Max Error (double-prec.) |
|---|---|---|
| Region 1 | $2.8\times10^{-7}$ | $8.7\times10^{-16}$ |
| Region 2 | $8.3\times10^{-5}$ | $5.3\times10^{-11}$ |
| Region $2^*_\delta$ | $8.8\times10^{-7}$ | $1.7\times10^{-15}$ |
| Region 3 | $9.3\times10^{-7}$ | $1.3\times10^{-15}$ |
| *(floating-point $\varepsilon$)* | $1.2\times10^{-7}$ | $2.2\times10^{-16}$ |

*Region 2 excluding a strip of width $\delta = 10^{-3}$ along the real axis.

**Table 3**. Empirical Error Bounds

## 7. Applications

Figures 12–14 show the result of some applications of the methods discussed. As noted in the introduction, conformal mapping from the disc to the square is not new and applications abound. The primary contribution of this work is the fast algorithms developed for computing the map and its inverse. Table 4 summarizes the running times for the various methods of computation. Note

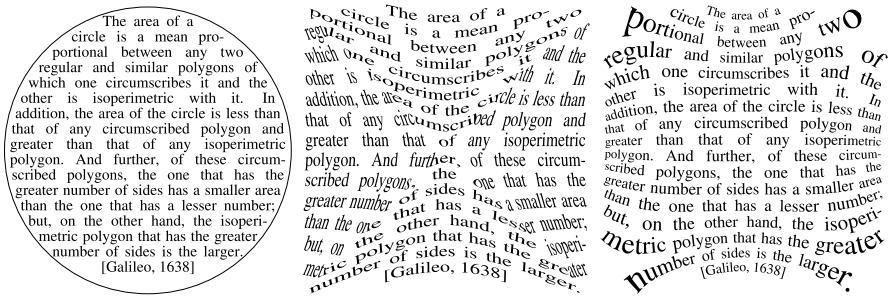


(a) (b) (c)

**Figure 12**. (a) Some text in a circle (homage to Knuth [Knuth 84]) transformed with (b) Shirley's map (note how obvious the discontinuties are) and the (c) conformal map. Note the extreme distortion in the corners.

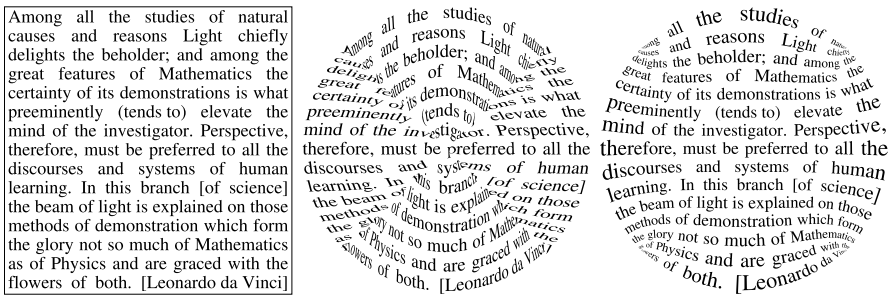


(a) (b) (c)

**Figure 13**. (a) Some text in a square transformed with (b) the inverse of Shirley's map and (c) the inverse conformal map. The distorion in the corners is noticeable, but most the text seems hardly affected.

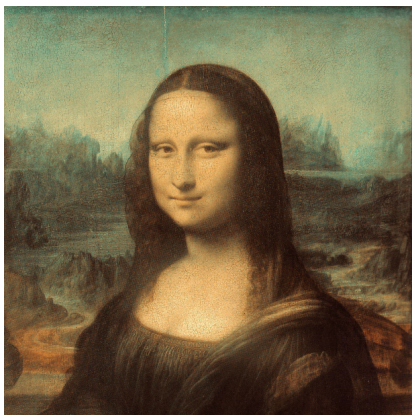

**Figure 14**. On some images, such as this famous portrait, the corner distortions of the conformal square-to-disc map are hardly noticable.

that the disc-to-square implementation runs only about 20% more slowly than Shirley's simple trigonometric map. The inverse map implementation is actually faster than that of Shirley's map. (The timings were performed on an Intel *Xeon* processor running at 3.2 GHz; the code was complied using GCC 4.1 under Linux kernel version 2.6.23.)

| Map Version | Forward (ms) | Inverse (ms) |
|---|---|---|
| Shirley's "Warp" Map | 258 | 299 |
| Complex Landen Ascending | 4259 | — |
| Complex AGM | 6709 | — |
| Real Landen Ascending | 5982 | — |
| Real Carlson | 2760 | — |
| Real Optimized AGM | 1010 | — |
| Series/Real Optimized AGM | 568 | — |
| Best Series/Real Optimized AGM | 303 | 214 |

**Table 4**. Time required for one million map function evaluations

## 8. Appendix

### *8.1. Computation of $q_n$*

The optimized AGM algorithm works with the tangents of angles rather than the angles directly. This complicates the determination of $q_n$, which tracks the branch of the inverse tangent. But because $q_n$ is an integer, incorrect values of $q_n$ cause errors in discrete steps: integer multiples of $\pi/(2^n a)$. If

$\tilde{F}(\phi)$ is a (separately computed) approximation to $F\big(\phi|\frac{1}{2}\big)$, then (15) implies

$$q_n \approx \frac{2^n a_n \tilde{F}\,(\phi) - \arctan(\tan\phi_n)}{\pi}. \tag{16}$$

Therefore, if $\tilde{F}(\phi)$ is within $\frac{1}{2}\,\pi/(2^n a_n)$ of $F\big(\phi|\frac{1}{2}\big)$, then $q_n$ can be computed by rounding the right-hand side of (16) to the nearest integer.

For $n = 4$ the allowable error, which is about 0.116 (for $|\phi| \leq \pi/2$) is large enough that even a rough linear approximation $F\big(\phi|\frac{1}{2}\big) \approx 1.14\phi$ suffices; in fact, $F\big(\phi|\frac{1}{2}\big) \approx \phi$ suffices for $|\phi| < 1.1$. A problem, though, is that the modified AGM algorithm starts with $\tan\phi_0$ rather than $\phi_0$—using the linear approximation requires an extra arctangent call to determine $\phi_0$. An approximation to the arctangent, combined with the linear approximation of $F$, can be used instead. For $|\phi| \leq 1.1$ (this is the largest value of $\phi$ that appears outside of Regions 1 and 2) either of the following approximations work:

$$\begin{aligned} F\big(\phi|\tfrac{1}{2}\big) &\approx \tan\phi - 0.193\,\tan^3\phi + 0.026\,\tan^5\phi, \\ &\approx \frac{\tan\phi}{1 + 0.172\,\tan^2\phi}. \end{aligned}$$

The maximum absolute errors for $|\phi| < 1.1$ are about 0.053 and 0.030, respectively, which are well within the allowable error of 0.116; in fact, these approximations actually suffice for $n \leq 5$, which is good for about 42 decimal digits. It is important to remember that the approximations may fail for $|\phi| > 1.1$.

### *8.2. Series Expansions Near the Diagonals*

As noted in Section 6, the transformation by $\xi$ given in (4.1) has a stability problem for $z$ near the real axis, i.e., when $z = x + i\,\delta$ for $\delta << x$. A direct series expansion mitigates that problem:

$$F\left(\frac{\pi}{2} - \arcsin(x + i\delta)\middle|\frac{1}{2}\right) \approx$$

$$F\left(\frac{\pi}{2} - \arcsin x\middle|\frac{1}{2}\right) - i\frac{\sqrt{2}\,\delta}{(1-x^4)^{1/2}} + \frac{\sqrt{2}\,x^3\delta^2}{(1-x^4)^{3/2}} + i\frac{\sqrt{2}\,(1+x^4)x^2\delta^3}{(1-x^4)^{5/2}}.$$

This approximation is only suitable if $\delta$ is small compared to $1-x$. A different series is needed for $x$ near 1 (and $y$ near 0): if $1 - z = x + i\,y$, then

$$F\left(\frac{\pi}{2} - \arcsin(x + i\,y)\middle|\frac{1}{2}\right) \approx \sqrt{x + i\,y}\left(1 + \tfrac{x+i\,y}{4} + \tfrac{11(x^2-y^2+2i\,xy)}{160} + \tfrac{x^3-3xy^2+i(3x^2y-y^3)}{128}\right).$$

(These formulas are applied *after* rotation by $\sqrt{i}$.)

### *8.3. Pseudocode*

This section contains pseudocode for the algorithms developed in this paper. Unless otherwise noted, all variables and values are complex.

**Function** `SumSeries(`$z$`,`$n$`)`

Compute $I(z)$ via the central power series of (14)
**input** : $z$, with $|z| < 1$; $n$, the number of terms to include
**output**: $I(z)$

$s \leftarrow z$; // *initialize the running series sum*
$p \leftarrow z$; // *initialize a running product*
**for** $k = 1 \ldots n$ **do**
  $p \leftarrow p\,z^4\,(2k-1)/(2k)$; // *$p$ now contains $(2k-1)!!/(2^k k!)\ z^{4k+1}$*
  $s \leftarrow s + p/(4k+1)$; // *add the term to the running sum*
**end**
**return** $s$;

**Function** `F(`$t$`)`

Compute $F\left(\phi|\frac{1}{2}\right)$ via the arithmetic-geometric mean.
**input** : $t = \tan\phi$, with $0 \le \phi < 1.1$ $(0 \le \tan\phi < 1.96)$
**output**: $F\left(\phi|\frac{1}{2}\right)$

// *All variables here are real*
$n \leftarrow 4$; // *(use $n \leftarrow 3$ for single-precision)*
$F_0 \leftarrow t - 0.193t^3 + 0.026t^5$; // $F_0 \approx F\left(\phi|\frac{1}{2}\right)$
$(a, b) \leftarrow (1, \sqrt{1/2})$; // *initialize the AGM pair*
**for** $k = 1 \ldots n$ **do**
  $t \leftarrow (a+b)t/(a-bt^2)$; // *compute* $\tan\phi_k$
  $(a, b) \leftarrow \left((a+b)/2,\ \sqrt{ab}\right)$; // *update the AGM pair*
**end**
$\phi_n \leftarrow \arctan(t)$;
**return** $\left(\phi_n + \pi\left\lfloor 0.5 + \left(2^n a F_0 - \phi_n\right)/\pi\right\rfloor\right)/(2^n a)$;

**Algorithm 1**. (Conformal Disc to Square Map.)

**input** : polar coordinates $[r, \theta]$ of a point in the unit disc:
$0 \le r \le 1$, $-\pi < \theta \le \pi$
**output**: rectangular coordinates $(x, y)$ of the point mapped conformally to the unit square: $-1 \le x, y \le 1$

**if** $r < r_0$ **then**
  // *Region 1: use the central power series*
  $z \leftarrow r\cos(\theta + \frac{\pi}{4}) + i\, r \sin\left(\theta + \frac{\pi}{4}\right)$;
  $w \leftarrow 2\sqrt{-i}/K$ `SumSeries`$(z, \lfloor 6.5/(1-r) - 2 \rfloor)$;
**else**
  // *Transform to Quadrant IV*
  $Q \leftarrow \lfloor \theta/(\pi/2) \rfloor + 1/2$ // *find the quadrant*
  $z \leftarrow r\cos\left(\theta - Q\frac{\pi}{2}\right) + i\, r \sin\left(\theta - Q\frac{\pi}{2}\right)$; // *rotate to Quadrant IV, and by* $\sqrt{i}$
  // *"Flip" to apply the power series, if possible*
  $\xi \leftarrow \sqrt{(1-z^2)/(1+z^2)}$;
  **if** $|\xi| < r_0$ **then**
    // *Region 2: use the power series on* $\xi$
    $w \leftarrow K/\sqrt{2} -$ `SumSeries`$(\xi, \lfloor 6.5/(1-|\xi|) - 2 \rfloor)$;
  **else**
    // *Region 3: use the AGM on real arguments as described in Section 3.4*
    // *all values except* $z$ *and* $w$ *are real*
    $(x, y) \leftarrow (\Re(z), \Im(z))$;
    $(A, B) \leftarrow \left(\sqrt{(x+1)^2 + y^2}, \sqrt{(x-1)^2 + y^2}\right)$;
    $(\alpha, \beta) \leftarrow \left(\frac{1}{2}(A+B), \frac{1}{2}(A-B)\right)$;
    $\gamma \leftarrow \alpha + \sqrt{\alpha^2 - 1}$;
    $T_\phi \leftarrow (1-\beta^2)/\beta^2$; // $T_\phi = \tan^2\phi$
    $b \leftarrow 2/T_\phi + (\gamma - 1/\gamma)^2/(4(1-\beta^2)) - 1$;
    $C_\lambda \leftarrow (b + \sqrt{b^2 + 8/T_\phi})/4$; // $C_\lambda = \cot^2\lambda$
    $T_\mu \leftarrow 2(T_\phi C_\lambda - 1)$; // $T_\mu = \tan^2\mu$
    $w \leftarrow K - \mathtt{F}\left(\sqrt{1/C_\lambda}\right) - i\,\mathtt{F}\left(\sqrt{T_\mu}\right)$;
    // *Adjust for the octant above the real axis*
    **if** $y > 0$ **then** $w \leftarrow \mathrm{conj}(w)$; // $\mathrm{conj}(w) \equiv \Re(w) - i\,\Im(w)$
  **end**
  // *Rotate back to the original quadrant, and scale by* $2\sqrt{-i}/K$
  // *(*$Q$ *contains the rotation by* $\sqrt{-i}$*)*
  $w \leftarrow 2w\,\left(\cos(Q\frac{\pi}{2}) + i\,\sin(Q\frac{\pi}{2})\right)/K$;
**end**
// $w$ *contains the rectangular coordinates of the mapped point*
$(x, y) \leftarrow (\Re(w), \Im(w))$;

**Acknowledgments.** The author wishes to thank Peter Shirley for pointing out the need for a fast disc-to-square conformal map implementation, and James Arvo for some helpful discussions on the subject. Of course, were it not for my complex analysis professors Marion Scheepers, David Ferguson, and M. Scott Osborne, this paper would not have been written.

## References

[Abramowitz and Stegun 64] Milton Abramowitz and Irene A. Stegun. *Handbook of Mathematical Functions with Formulas, Graphs, and Mathematical Tables*, ninth Dover printing, tenth GPO printing edition. New York: Dover, 1964.

[Churchill and Brown 90] Ruel V. Churchill and James Ward Brown. *Complex Variables and Applications*, Sixth edition. New York: McGraw-Hill, 1990.

[Grattan-Guinness 03] Ivor Grattan-Guinness, editor. *Companion Encyclopedia of the History and Philosophy of the Mathematical Sciences*. Baltimore, MD: Johns Hopkins University Press, 2003.

[Knuth 84] D. E. Knuth. *The TEXBook*. Reading, MA: Addison-Wesley, 1984.

[Needham 99] Tristan Needham. *Visual Complex Analysis*. New York: Oxford University Press, 1999.

[Press et al. 92] William H. Press, Saul A. Teukolsky, William T. Vetterling, and Brian P. Flannery. *Numerical Recipes in C: The Art of Scientific Computing*, Second edition. New York: Cambridge University Press, 1992.

[Shirley and Chiu 97] Peter S. Shirley and Kenneth Chiu. "A Low Distortion Map Between Disk and Square." *journal of graphics tools* 2:3 (1997), 45–52.

[Spiegel 64] Murray Spiegel. *Schaum's Outlines: Complex Variables (With an Introduction to Conformal Mapping and Its Applications)*. New York: McGraw-Hill, 1964.

## Web Information:

http://jgt.akpeters.com/papers/Stark09_2/

Michael M. Stark, Computer Science Department, College of Engineering, Boise State University, 1910 University Drive Boise, ID 83725 (stark@cs.boisestate.edu)

Received February 12, 2009; accepted in revised form July 21, 2009.